12-1-2021

# Investigating Strike-Slip Faulting Parallel to the Icelandic Plate Boundary Using Boundary Element Models

Anna E.R. Pearson
*Smith College*

John P. Loveless
*Smith College*, jloveles@smith.edu

Tectonics®

RESEARCH ARTICLE
10.1029/2021TC007002

# Investigating Strike-Slip Faulting Parallel to the Icelandic Plate Boundary Using Boundary Element Models

**Anna E. R. Pearson**[1,2] **and John P. Loveless**[1]

[1]Department of Geosciences, Smith College, Northampton, MA, USA, [2]Now at Kentucky Geological Survey, Lexington, KY, USA

**Key Points:**

- Many rift-parallel faults in Iceland show oblique or strike slip instead of the expected normal slip
- Boundary element modeling reproduces this unexpected slip based on mechanical interactions between rifting, the hotspot, and faults
- Modeling supports additional possible impacts from stress permutations and dike intrusion

**Supporting Information:**

Supporting Information may be found in the online version of this article.

**Correspondence to:**

A. E. R. Pearson,
aerpearson@gmail.com

**Citation:**

Pearson, A. E. R., & Loveless, J. P. (2021). Investigating strike-slip faulting parallel to the Icelandic plate boundary using boundary element models. *Tectonics*, *40*, e2021TC007002. https://doi.org/10.1029/2021TC007002

Received 22 JUL 2021
Accepted 23 NOV 2021
Corrected 8 JAN 2022

The article was corrected on 8 JAN 2022. See the end of the full text for details.

**Abstract** Most faults in Iceland strike roughly parallel to the divergent plate boundary, a part of the North American-Eurasian plate boundary, which would be expected to lead to primarily normal faulting. However, several studies have observed a significant component of rift-parallel strike-slip faulting in Iceland. To investigate these fault kinematics, we use the boundary element method to model fault slip and crustal stress patterns of the Icelandic tectonic system, including a spherical hotspot and uniaxial stress that represents rifting. On a network of faults, we estimate the slip required to relieve traction imposed by hotspot inflation and remote rifting stress and compare the model results with observed slip kinematics, crustal seismicity, and geodetic data. We note a good fit between model-predicted and observed deformation metrics, with both indicating significant components of normal and strike-slip faulting and consistency between recent data and longer-term records of geologic fault slip. Possible stress permutations between steeply plunging $\sigma_1$ and $\sigma_2$ axes are common in our models, suggesting that localized stress perturbations may impact strike-slip faulting. Some increases in model complexity, including older hotspot configurations and allowing fault opening to simulate dike intrusion, show improvement to model fit in select regions. This work provides new insight into the physical mechanisms driving faulting styles within Iceland away from the current active plate boundary, implying that a significant portion of observed strike-slip faulting is likely caused by the combined effects of tectonic rifting, hotspot impacts, and mechanical interactions across the fault network.

**Plain Language Summary** Faulting in Iceland is expected to be mostly normal faulting, which is characteristic of a divergent tectonic environment. However, several studies have found substantial strike-slip faulting. To try to understand the causes of this unexpected pattern, we create a model that represents the main features of the tectonic environment in Iceland. This includes a three-dimensional representation of the faults associated with the tectonic plate boundary that runs through Iceland, across which two tectonic plates are pulling apart from each other, and a hotspot underneath. We find that this model can explain a large part of that unexpected strike-slip faulting, along with identifying potential additional complexity from other processes. This provides new information that is important to understanding faulting in Iceland and possibly also other similar tectonic environments.

## 1. Introduction

Faults in Iceland mainly strike subparallel to the active rift zone (Figure 1) and are dominated by normal faulting in the active rift zones as well as strike-slip faulting in the major transform zones (Karson et al., 2018). Surprisingly, widespread rift-parallel strike-slip and oblique slip faulting have also been found outside the active transform zones (Bergerat et al., 2000; Gudmundsson et al., 1992; Karson et al., 2018; Plateaux et al., 2012). This presents a curious feature of faulting kinematics in the region as, in a divergent setting, primarily normal slip is expected on faults that strike parallel to the boundary.

### 1.1. Tectonic Setting

A combination of rifting and hotspot processes has allowed Iceland to form above the North American–Eurasian plate boundary, creating an unusual and dynamic geologic setting with high volcanic and seismic activity. Active rift zones strike NNE to SSW through the island, across which the North American and Eurasian plates diverge along a 105° azimuth with a spreading rate of about 18.4 mm/year (DeMets et al., 1994). The active rift zones are connected by two transform fault zones, the South Iceland Seismic Zone (SIZ) in Southern Iceland and the Tjörnes Fracture Zone (TFZ) in Northern Iceland, as well as further north and south by several oblique

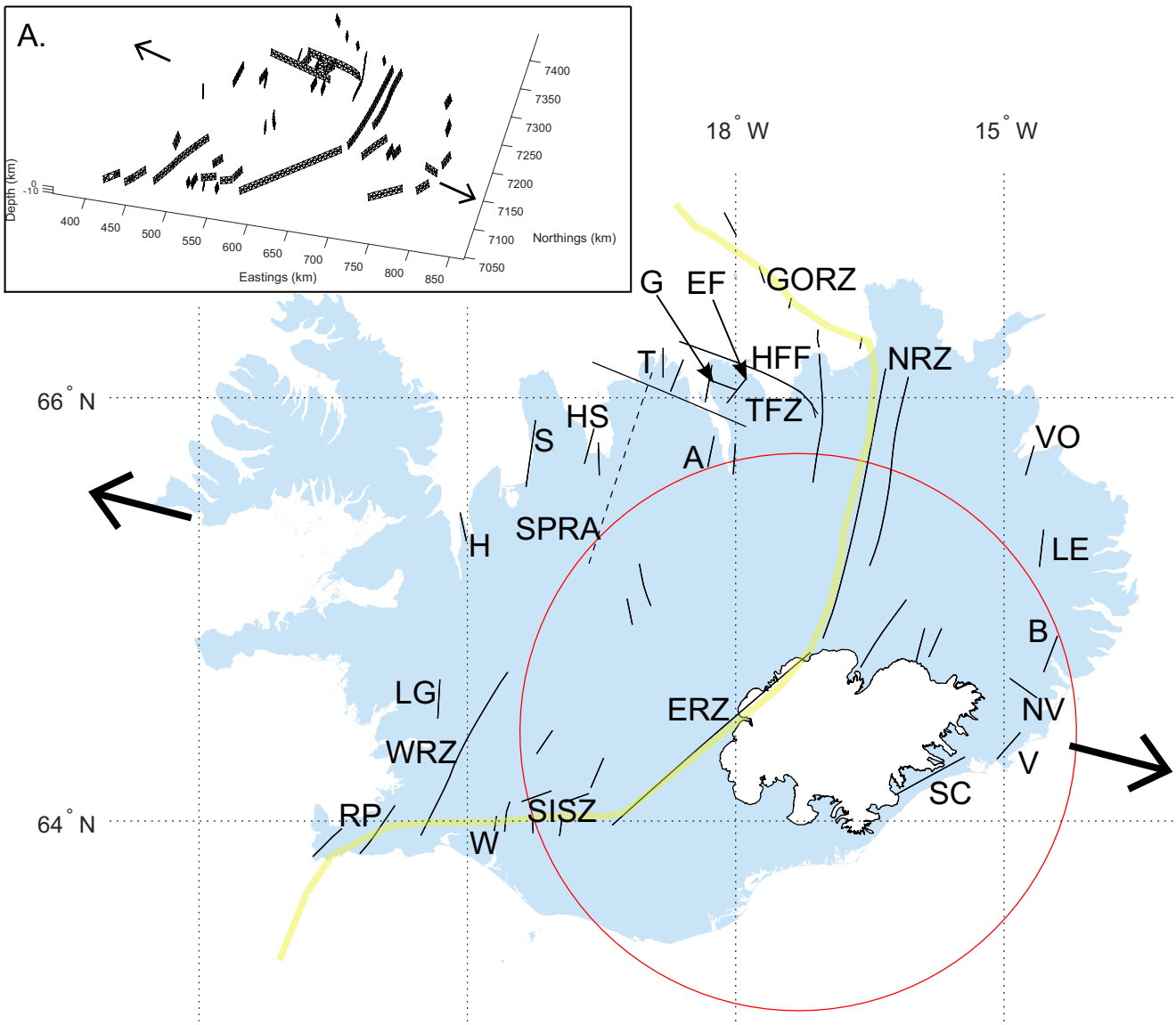


**Figure 1.** Map identifying major faulting zones in Iceland and other areas referenced in the text and used in the model, clockwise from the northwest as follows: H (Heggstaðanes), S (Skagi), SPRA (Skagafjördur paleo-rift axis, dashed line, inactive), HS (Hegranes), T (Tröllaskagi), A (Akureyri), G (Grenivík), EF (East Flateyjarskagi), TFZ (Tjörnes Fracture Zone), HFF (Húsavík-Flatey Fault), GORZ (Grímsey Oblique Rift Zone), NRZ (Northern Rift Zone), VO (Vopnafjörður), LE (Lagarfljót-Eiðar), B (Berufjörður), NV (Northeast Vestrahorn), V( Vestrahorn), SC (Southeast Coast), ERZ (Eastern Rift Zone), SISZ (South Iceland Seismic Zone, Hreppar area), W (Western Hreppar), WRZ (Western Rift Zone), LG (Langavatn-Gljúfurá), and RP (Reykjanes Peninsula). The fault traces shown are used as model inputs (see 3D perspective of fault meshes in 1a). The hotspot is shown as a red circle (also used as a model input), Vatnajökull is shown in white (Sigurdsson, 2005), and arrows represent the direction of rifting (DeMets et al., 1994).

rifting zones, including the Grímsey Oblique Rift Zone (GORZ) and the Reykjanes Peninsula (RP; Figure 1; Einarsson, 2008). Rifting in Iceland can serve as an important analog to better understand faulting processes at mid-ocean ridges, as it is difficult to observe processes on the seafloor (Karson et al., 2018). Iceland is underlain by a hotspot, which is generally identified as centered beneath the Vatnajökull Ice Cap (Figure 1), with models of the proposed mantle plume varying in radius, temperature, and structure (Hanan & Schilling, 1997; Martin et al., 2011; Wolfe et al., 1997).

Iceland faces a significant seismic hazard due to the combination of rifting and hotspot processes, with earthquakes in the SISZ and the TFZ reaching a maximum of M7 and having caused considerable damage (Árnadóttir et al., 2009; Einarsson, 2008). Significant historical earthquakes have been focused along the plate boundaries, especially the SISZ and the TFZ, as well as near volcanic centers (J. Ö. Bjarnason et al., 2016). However, due

to the complexity of the tectonic setting, there is a lack of understanding of the physical mechanisms that drive faulting styles within Iceland away from the current active plate boundary.

### 1.2. Faulting Kinematics and Complexities

Faults in Iceland dominantly strike subparallel to the active rift zone, with seismicity reaching maximum depths of 15–20 km (Björnsson, 2008). Normal faulting and rift-parallel fissure swarms are common, particularly within the major rift zones (Einarsson, 2008; Hjartardóttir et al., 2015). Slip data collected from outside the active transform zones show widespread strike-slip faulting, including on faults that strike parallel to the rift zones (Bergerat et al., 2000; Gudmundsson et al., 1992; Karson et al., 2018; Plateaux et al., 2012). Strike-slip faults outside the active rift zones also commonly strike parallel to nearby dikes, suggesting that they are likely similarly parallel to the active rift zone at the time of formation (Karson, 2017). Slip data within the Karson et al. (2018) and Plateaux et al. (2012) data sets document normal, oblique, and strike-slip faulting over a wide region, including many conjugate strike-slip faults. These studies also identify similarly oriented axes of maximum extension for both strike-slip and normal faults, indicating that the strike-slip faults are likely also related to rifting (Plateaux et al., 2012). Constraints on ages of faulting are limited to mostly occurring within the last 9–11 Myr since much of the bedrock is 9 Ma or older, leaving few significant and consistent cross-cutting relationships other than the constraint that faulting must have occurred after the rock formed (Karson et al., 2018). However, patterns of multiple sets of slickenlines, representing a shift between normal and strike-slip faulting, while rare, are present within the data and some faults do cut historic lavas, which indicates that some slip is relatively modern (Karson et al., 2018).

Previous work has proposed a variety of additional mechanisms and complexities to explain the unanticipated pattern of rift-parallel strike-slip faulting outside the active transform zones (Gudmundsson et al., 2009; Karson et al., 2018; Plateaux et al., 2012). Interaction between hotspot inflation and rifting processes may create a more oblique component of slip than would be expected solely due to rifting. The crust in Iceland is also highly anisotropic, with many overlapping sets of old faults, fissures, and dikes (Karson et al., 2018). Anisotropic crust has been suggested as a primary property that favors stress permutations, in which the orientations of two principal stresses exchange places from one locale to another, usually due to variation in vertical loading, which has been proposed to explain coexisting normal and strike-slip faults in many areas of Iceland and around the world (Hu & Angelier, 2004; Plateaux et al., 2012). In addition, Iceland seems to be currently undergoing a rift jump, abandoning the Western Rift Zone and transferring the rifting process to the Eastern Rift Zone, with rift propagation away from the hotspot, which is suggested as an additional factor driving strike-slip faulting (Einarsson, 2008; Karson, 2017). Propagation of the Northern Rift Zone to the north and the Eastern Rift Zone to the south is proposed to cause crustal block rotations, which result in strike-slip faulting on rift-parallel faults (Karson, 2017). Previous rift jumps may also have led to the abandonment of former oblique spreading zones, with at least one former spreading zone identified along Skagafjördur (Figure 1; Garcia et al., 2008; Hardarson et al., 1997). Observing these areas today would then lead to the identification of strike-slip faulting far from modern oblique spreading or transform zones (Karson et al., 2018). Finally, the combination of dike intrusion and tensile rifting stress has been implicated in sinistral and dextral faulting subparallel to the tips of dikes in a diverse set of locations (Ágústsdóttir et al., 2016; Gudmundsson et al., 2009; Hjartardóttir et al., 2009 as cited in Plateaux et al., 2012). The use of finite element models has also indicated north-south trending zones of high shear stress between adjacent volcanic systems as a result of dike intrusions into each of the adjacent systems, leading to both dextral and sinistral strike-slip faulting (Gudmundsson et al., 2009).

Our modeling focuses on investigating many mechanisms proposed within the literature to explain the prevalence of strike-slip faulting in Iceland. We evaluate our boundary element modeling by comparing results to fault slip, seismicity, and deformation data. We use modeling to consider how the fault slip and crustal stress patterns in Iceland relate to mechanical fault–hotspot interactions and possible additional influences, including stress permutations, dike-induced faulting, rift propagation, and abandoned spreading zones.

## 2. Methods

### 2.1. Model Structure and Evaluation

Modeling for this project is primarily done using *tribemx* (Delano et al., 2017; Loveless, 2019; Thomas, 1993), an elastic boundary element method program, in which faulting processes can be simulated by embedding triangular

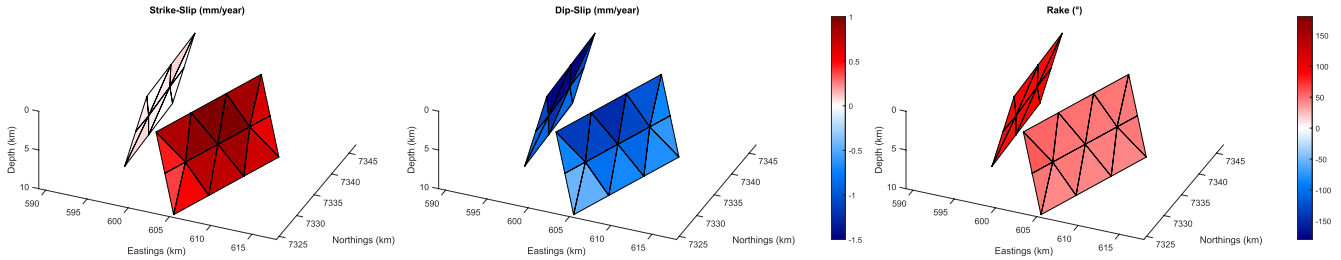


**Figure 2.** Figure showing example slip distribution results for faults in the Tröllaskagi area for the best fit parameters (hotspot contribution of 110 mm/year, rifting azimuth of 115°). Strike-slip results are shown such that negative corresponds to dextral movement and dip-slip results are shown such that negative corresponds to normal movement.

dislocation elements (TDEs) within a homogeneous elastic half-space. In these models, a traction or slip boundary condition is specified in the strike-parallel, dip-parallel, and element-normal direction on each TDE, and we specifically assume that faults have no shear traction and no element-normal slip, except as described in Section 2.3. The program projects the stress imposed by simulated tectonic inputs onto the element geometry, creating a set of traction vectors for each element, then solves for the slip distribution required to relieve the shear traction imposed by the applied stress, considering interaction among the different faults (Cooke & Dair, 2011). We also calculate stress and strain tensor components and displacement (velocity) vectors at off-fault observation coordinates.

We defined our standard model of fault geometry by combining a geologic map of Iceland (Jóhannesson, 2014), a representative sample of the areas of strike-slip faulting identified by Karson et al. (2018), and several additional detailed fault maps (Bergerat et al., 2000; Rögnvaldsson et al., 1998). Fault map coverage throughout Iceland is highly variable, necessitating a generalize model based on available data. We modeled the three-dimensional geometry of faults by projecting their surface traces to 10 km depth, then rotating to an average dip of the directly associated fault region in the Karson et al. (2018) data or, for faults not included in that data set, a dip of 70°, reflecting patterns of slightly steeper dips found in the Karson et al. (2018) data than predicted for normal faults (Anderson, 1905). Each fault was then meshed as a contiguous network of TDEs using the open-source program *Gmsh* (Geuzaine & Remacle, 2009). The hotspot was incorporated as a hollow sphere with the surface discretized as a network of TDEs, with a radius of 150 km and a top surface at a depth of 100 km centered under the Vatnajökull Ice Cap (circle in Figure 1, mesh shown in Figure S1 in Supporting Information S1; I. Bjarnason, 2008; Morgan & Morgan, 2007; Wolfe et al., 1997). On these TDEs, we apply element-normal dislocation to simulate inflation. We model rifting as a uniaxial axis of tension along an azimuth of relative plate motion (Figure 1), at a magnitude of $6 \times 10^6$ Pa/year, which is similar in magnitude to estimates of remote stress as calculated based on a best fitting horizontal strain rate tensor derived from regional GPS velocities (Cardozo & Allmendinger, 2009; Árnadóttir et al., 2009) and Lamé parameters of $3 \times 10^{10}$ Pa. This applied remote stress, as well as stress arising from the element-normal dislocations on hotspot TDEs, is projected onto fault TDEs as traction vectors. The output slip distribution on each modeled fault (e.g., Figure 2), calculated such that the imposed shear traction is completely relieved, is used as a basis for characterizing fault kinematics described by the model. From the fault slip distributions and calculations of total stress, strain, and displacement rates at specified coordinates within the elastic medium, we calculate moment tensor, principal stress, and principal strain rate axes. These axes are used to evaluate the model results, comparing the model output with existing sets of fault slip, seismicity, and crustal deformation data in different regions of Iceland (Figure 3), representing the goodness-of-fit of the model to the data as a set of angular differences in axis orientations.

First, we consider comparison with moment tensor axes (pressure [P] and tension [T] axes) calculated from field measurements of fault slip (Karson et al., 2018) and from earthquakes within the Global Centroid Moment Tensor (CMT) data set (Dziewonski et al., 1981; Ekström et al., 2012). For the fault slip records, we used the *FaultKin* program (Allmendinger et al., 2011; Marrett & Allmendinger, 1990) to derive P and T axes from the strikes, dips, slip sense, and striae trends and plunges in the records (Karson et al., 2018), using all reported measurements at a listed field site to give a single set of best fit axes for that site. We compared the data to a single set of kinematic axes for each modeled fault corresponding to a listed field area in the Karson et al. (2018) data set, calculated using the modeled slip distribution output in the *MomTens* MATLAB function, with the results weighted based

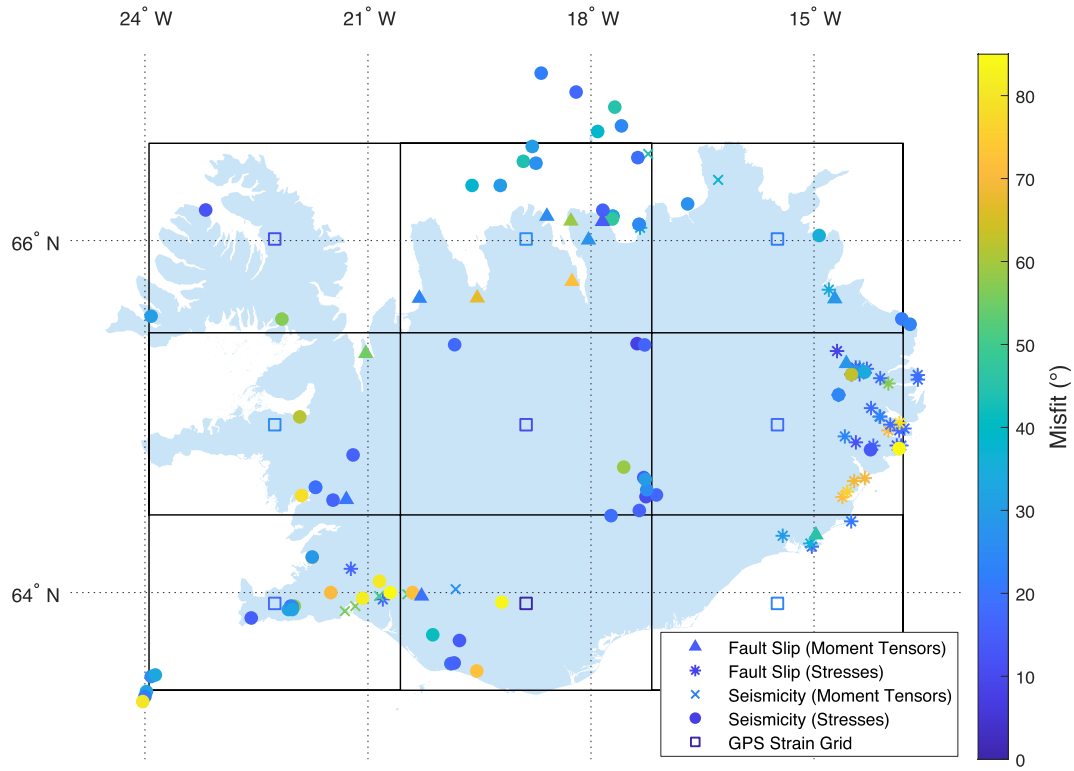


**Figure 3.** Map of angular misfit of the reference parameters with each comparison data point in the appropriate reference listed in the following, including moment tensor data derived from fault slip (triangles; Karson et al., 2018), principal stress data derived from fault slip (asterisks; Bergerat et al., 1990; Gudmundsson et al., 1992; Plateaux et al., 2012), moment tensors from seismicity (crosses; Dziewonski et al., 1981; Ekström et al., 2012), principal stresses from seismicity (circles; Ziegler et al., 2016), and the grid of regions compared with GPS data (open squares placed at the center of each of the nine regions noted by the solid black grid; Árnadóttir et al., 2009).

on slip magnitude (Cardozo in Allmendinger et al., 2011). For the CMT data, we used the *MomTens* function to derive moment tensor axes from fault plane solutions available in the Global CMT data set (Cardozo in Allmendinger et al., 2011; Dziewonski et al., 1981; Ekström et al., 2012), which we compared to principal axes of modeled strain tensors at each earthquake hypocenter. We eliminated from our comparison any earthquakes from the CMT data set that were located close to the center of the hotspot, the site of several major volcanoes including Grímsvötn and Bárðarbunga. These earthquakes were eliminated due to a tendency for northeast-trending T axes, a difference that we interpret to be from localized influence of those volcanoes, which we do not consider within our model. When calculating the overall misfit between modeled and reported kinematic axis orientations for the CMTs, we weighted each of the angular differences based on the seismic moment of the associated earthquake.

We also consider principal stress axes derived from field measurements of fault slip (Bergerat et al., 1990; Gudmundsson et al., 1992; Plateaux et al., 2012) and local crustal earthquakes from the Iceland Meteorological Office (IMO) catalog (Ziegler et al., 2016), which we compare directly with principal axes from model stress tensors calculated at the reported measurement or hypocenter sites. We also allow for the possibility of stress permutations based on similarity in orientation of observed and modeled axes. Previous work has identified permutations between steeply plunging $\sigma_1$ and $\sigma_2$ as a possible reason for strike-slip faulting in Iceland, as extensional settings with a high deviatoric stress ratio can cause permutations between steeply plunging $\sigma_1$ and $\sigma_2$ axes that correspond to conjugate normal and strike-slip faults, respectively (Figure 4; Hu & Angelier, 2004; Plateaux et al., 2012). In particular, key processes favoring stress permutations include anisotropy in the crust as a result of folding and faulting as well as elastic rebound, potentially as part of deglaciation (Hu & Angelier, 2004; Plateaux et al., 2012). We note a possible stress permutation at sites where exchanging a pair of modeled principal axis orientations yields a misfit that is lower and is less than 50° for both of those axes, also noting the stress ratio, defined as $\Phi = (\sigma_2 - \sigma_3)/(\sigma_1 - \sigma_3)$ based on the deviatoric stresses, as further evidence supporting the possibility

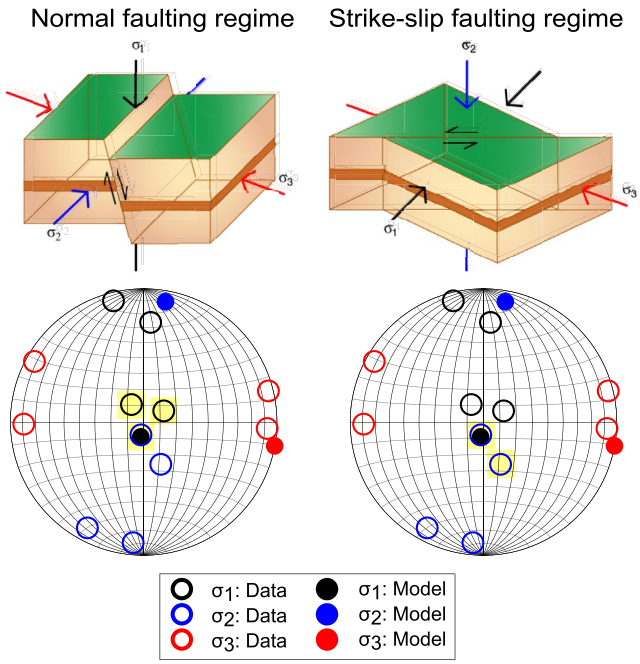


**Figure 4.** Figure demonstrating stress permutations, showing characteristic orientations of principal stress axes for a normal faulting regime on the left and a strike-slip faulting regime on the right. Stress states differ only by flipping the orientations of $\sigma_1$ and $\sigma_2$, which can occur due to a small change in magnitudes of the principal stresses. The stereonets show selected results from our model using the best fit model results and comparison data for the Húsavík-Flatey Fault, with several examples of steeply plunging $\sigma_1$ axes highlighted in yellow on the left and steeply plunging $\sigma_2$ axes highlighted on the right.

of a stress permutation. In other words, we consider the model to represent a good fit to data in places where the modeled $\sigma_1$ is similar in orientation to the observed $\sigma_2$ and vice versa.

Finally, we evaluate model predictions based on principal horizontal strain rate axes calculated from GPS velocity data throughout Iceland from 1993 to 2004 in a local reference frame (Árnadóttir et al., 2009; Cardozo & Allmendinger, 2009). We calculate velocity vectors at the GPS station locations, which arise from the remote stress representing rifting, simulated inflation of the hotspot, and slip on the modeled faults. We then use the nearest neighbor method to find the best fitting horizontal strain rate tensors for the stations in each of nine regions across Iceland using the *GridStrain* MATLAB function (Cardozo in Allmendinger et al., 2011), comparing the maximum principal extension rate axes from the observed and modeled velocities.

As each type of comparison data can be expressed as a set of orientations, we use angular misfit criteria to define the goodness-of-fit of model results to the data sets. For moment tensor and principal stress axes, there are two independent axes, so the average angular misfit at each fault or observation point is defined as the average of the angular misfit for the two axes (P and T axes for the moment tensors and $\sigma_1$ and $\sigma_3$ axes for the principal stresses). For horizontal principal strain rate axes derived from GPS velocities, there is only one independent axis, so the angular misfit is defined as the misfit between the observed and modeled maximum extension rate axis.

### 2.2. Standard Model Parameters

The tectonic inputs to our boundary element models include a stress tensor that represents rifting and element-normal dislocation applied to the hotspot to represent its inflation. While global tectonic models (DeMets et al., 1994) suggest an azimuth of rifting of 105°, we explore a range of possibilities. We term our standard parameter range as a set of candidate rifting azimuths and hotspot dislocation rates. We constructed a series of trials varying the remote stress tensor representing the rifting between the two plates as uniaxial tension along a prescribed azimuth in 5° increments from 0° to 180° (keeping the stress rate constant at $6 \times 10^6$ Pa/year), along with a variable contribution from the hotspot based on element-normal dislocation to represent inflation, from 0 to 200 mm/year. For comparison with all available data, we define the reported misfit for each trial as a simple unweighted average of the average angular misfits to the two fault slip data sets, two earthquake data sets, and single GPS-derived strain rate data set.

### 2.3. Additional Variations to Model Parameters

We tested several variations to the standard model parameters to see whether slip patterns observed in some areas of Iceland may be emblematic of the impact of additional processes, focusing on comparing the model results to the moment tensor data derived from fault slip (Karson et al., 2018). We tested variability in the location of the modeled hotspot while holding its diameter and depth constant, incrementally varying the location between the assumed modern location and a proposed location at 6 Ma (Figure S9 in Supporting Information S1; I. Bjarnason, 2008; Martin et al., 2011). We ran this set of trials for each parameter pair from the top 5% of trials within the standard parameter range, ranked by angular misfit, and averaged the results. As an additional test, we also expanded the fault map to include the Skagafjördur paleo-rift axis (SPRA) in northwest Iceland (Figure 1) along with an adjusted hotspot location, as previous work has suggested active rifting along that axis from 8 to 2.8 Ma, so some observed faulting in the area could be related to a now abandoned oblique spreading zone (Garcia et al., 2003; Hjartarson, 2003). For this model, we also removed the Dalvík Lineament from the fault map, as it overlaps with the proposed location of the paleo-rift axis.

To test rift propagation as a proposed explanation for strike-slip faulting in Iceland, a process which results in less finite spreading at the propagating rift tips (Karson et al., 2018), we implemented a variable magnitude of

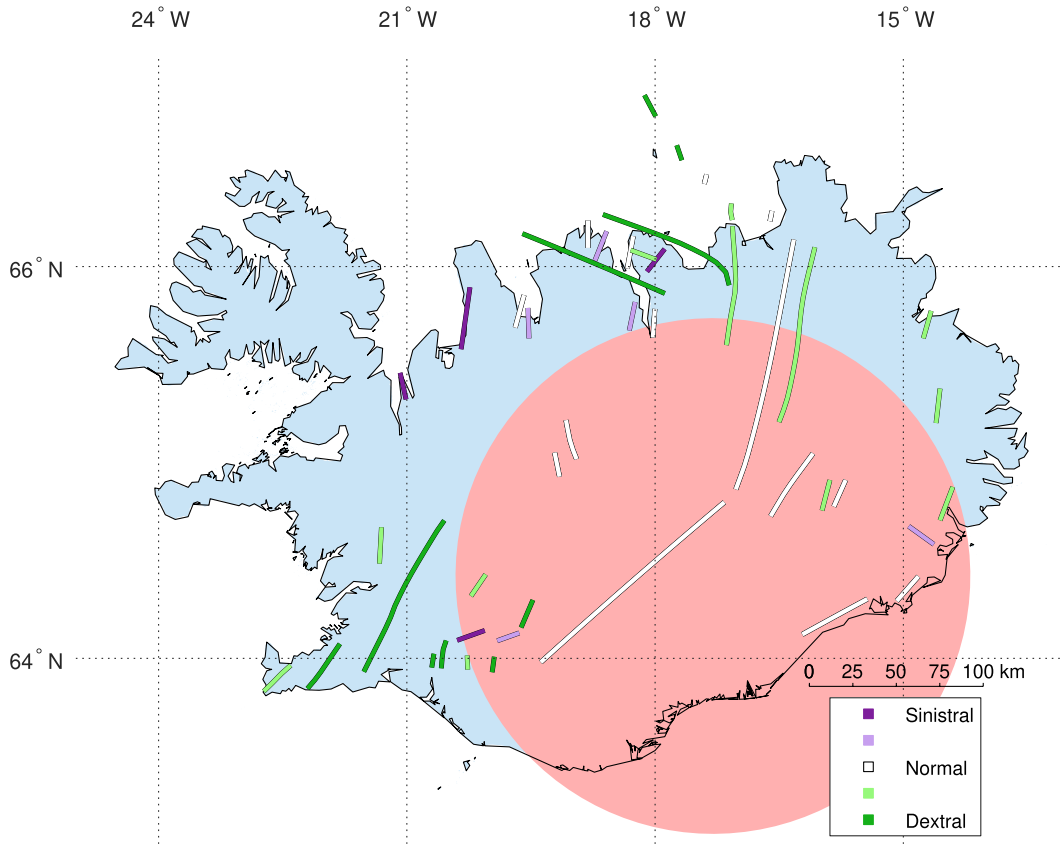


**Figure 5.** Map showing rake patterns across each fault in the model for the reference parameters, based on the average rake across all elements of the fault and weighted by slip magnitude.

uniaxial remote stress to simulate varying intensity of rifting across Iceland. We projected the variable remote stress onto the element geometry directly, weighting the remote stress to be progressively smaller based on the distance from the center of the hotspot (at the site of the nonpropagating rift tips), and then solved for slip needed to relieve the imposed traction as in the standard model. Spatially variable weights were normalized between 0 and 1, with the maximum remote stress close to the center of the hotspot.

As a method of simulating dike intrusion, we allow the fault TDEs themselves to open (or close) by moving in an element-normal direction, in addition to slipping parallel to their strike and dip. By allowing some of the plate boundary-perpendicular motion to be taken up by opening similar to the formation of dikes, the slip on the faults could potentially be more strike slip dominated. We tested this method by allowing all faults to open or allowing opening only on faults that are poorly fit by the reference model. We define poorly fit faults as those with an angular misfit above 35°.

## 3. Results

### 3.1. Evaluation of Standard Model

Under the standard model, the parameters that yield the lowest average angular misfit across all data sets (29.4°) were a rifting azimuth of 115° with 110 mm/year of element-normal dislocation on the hotspot. We define these as the reference parameters. The distribution of fault rakes represents the basic set of model results (full stereonet results are shown in Figures S2–S7 in Supporting Information S1). The reference model rake pattern (averaged for each fault, weighted by slip magnitude) shows a widespread mix of normal and strike-slip faulting kinematics, most commonly sinistral slip in the northwest of Iceland and dextral slip in the northeast and southwest (Figure 5).

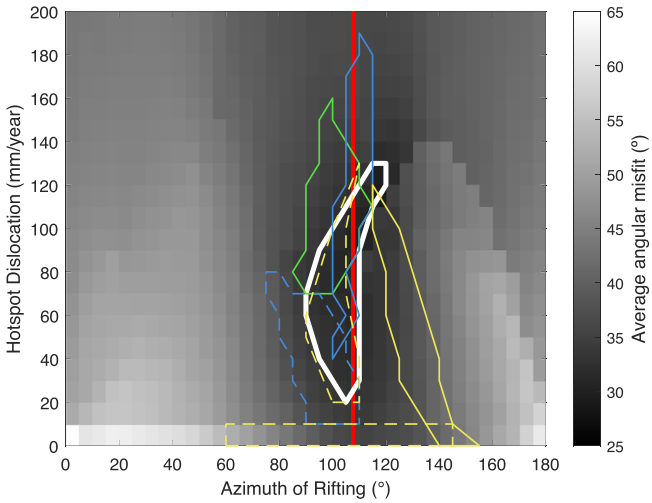


**Figure 6.** Angular misfit for all data for each trial in the standard parameter range. Red line identifies the rifting azimuth predicted by NUVEL 1-A, white line denotes the top 5% of trials in terms of minimized misfit. Best fit regions in comparison with each of the individual data sets are shown as follows: moment tensors derived from fault slip (solid blue; Karson et al., 2018), principal stresses derived from fault slip (dashed blue; Bergerat et al., 1990; Gudmundsson et al., 1992; Plateaux et al., 2012), Centroid Moment Tensor (CMT) data (solid yellow; Dziewonski et al., 1981; Ekström et al., 2012), Iceland Meteorological Office (IMO) data (dashed yellow; Ziegler et al., 2016), and GPS data (green; Árnadóttir et al., 2009).

We note similarly good fits to the data sets for the parameter pairs that define the top 5% of trials within the standard parameter range, ranked in terms of average angular misfit (white polygon, Figure 6). These pairs feature rifting azimuths between 90° and 120° and a hotspot contribution between 20 and 130 mm/year. We find substantial overlap in the parameter pairs that yield the top 5% of trials when compared to each individual data set; the principal stress data sets show best fit trials at a lower hotspot contribution (colored polygons, Figure 6; Bergerat et al., 1990; Gudmundsson et al., 1992; Plateaux et al., 2012; Ziegler et al., 2016). Table 1 summarizes the model parameters that best fit each individual data set.

Some variability between the top 5% of trials fitting individual data sets can be seen (Figures 6 and S8). In particular, in comparing modeled moment tensor axes with those determined from the fault slip data published in Karson et al. (2018), we find consistency with the reference parameters, although this data set is better fit with a higher hotspot influence (Figure S8 in Supporting Information S1). Using the reference parameters, the average angular misfit is only 0.7° higher than the model that best fits the individual data set (37.5° vs. 36.8°), which uses 50 mm/year of hotspot dislocation and a rifting azimuth of 105°, and is only poorly fit in the regions of Heggstaðanes, Vestrahorn, and a cluster in north central Iceland of Grenivík, Hegranes, and Akureyri (Figures 1 and 3). As compared to a trial with the same rifting azimuth of 115° but no hotspot contribution, the modeled fault slip shows increased strike-slip motion on the Húsavík-Flatey Fault and in the areas of Vopnafjörður, Berufjörður, the Flateyjarskagi Peninsula, and Hreppar, along with decreased strike-slip motion in southeast Iceland and Akureyri. The trial with hotspot influence also shows greater sinistral as opposed to dextral strike-slip faulting in northwest Iceland.

For the CMT data alone (Dziewonski et al., 1981; Ekström et al., 2012), the top 5% of trials within the standard parameter range show a covariance between rifting azimuth and hotspot contribution, with an azimuth of rifting more consistent with the reference parameters associated with a higher hotspot contribution (Figure 6 and Figure S8 in Supporting Information S1). Using the reference parameters, the average angular misfit is only 0.5° higher than the model that best fits the CMT data alone (26.9° vs. 26.4°) and the highest misfits for both were found in the western part of the Hreppar area (Figure 3). Tension axes are more southerly trending on the RP and in the Hreppar area in southwest Iceland for both the model and observed data.

We find that the best fitting trials to the principal stress data derived from fault slip (Bergerat et al., 1990; Gudmundsson et al., 1992; Plateaux et al., 2012) are largely consistent with the reference parameters but feature a slightly lower hotspot contribution. Northeast Vestrahorn (Figures 1 and 3) is the site of the majority of the improvement in misfit between the reference parameters, which have a misfit of 32.7°, and the best fit parameters to the individual data set, with a misfit of 21.2° at 20 mm/year of hotspot contribution and a rifting azimuth of

**Table 1**
*Table Showing Lowest Average Angular Misfit in Comparison With Each of the Comparison Data Sets and the Overall Data, for the Standard Model*

| | Fault slip derived (moment tensor axes, $n = 13$) | | | Fault slip derived (stress tensor axes, $n = 36$) | | | GPS derived (principal strain axes, $n = 9$) | | | Focal mechanism derived (moment tensor axes, $n = 13$) | | | Focal mechanism derived (stress tensor axes, $n = 82$) | | | Overall | | |
|---|---|---|---|---|---|---|---|---|---|---|---|---|---|---|---|---|---|---|
| | H | R (°) | M (°) | H | R (°) | M (°) | H | R (°) | M (°) | H | R (°) | M (°) | H | R (°) | M (°) | H | R (°) | M (°) |
| Best fit | 50 | 105 | 36.8 | 20 | 95 | 21.2 | 90 | 105 | 13.6 | 90 | 120 | 26.4 | 0 | 125 | 38.3 | 110 | 115 | 29.4 |
| Reference parameters | 110 | 115 | 37.5 | 110 | 115 | 32.7 | 110 | 115 | 17.1 | 110 | 115 | 26.9 | 110 | 115 | 41.8 | | | |

*Note*. The second row shows the misfit in comparison to each data set for the trial following the reference parameters (H, hotspot contribution [mm/year]; R, rifting azimuth; M, average angular misfit).

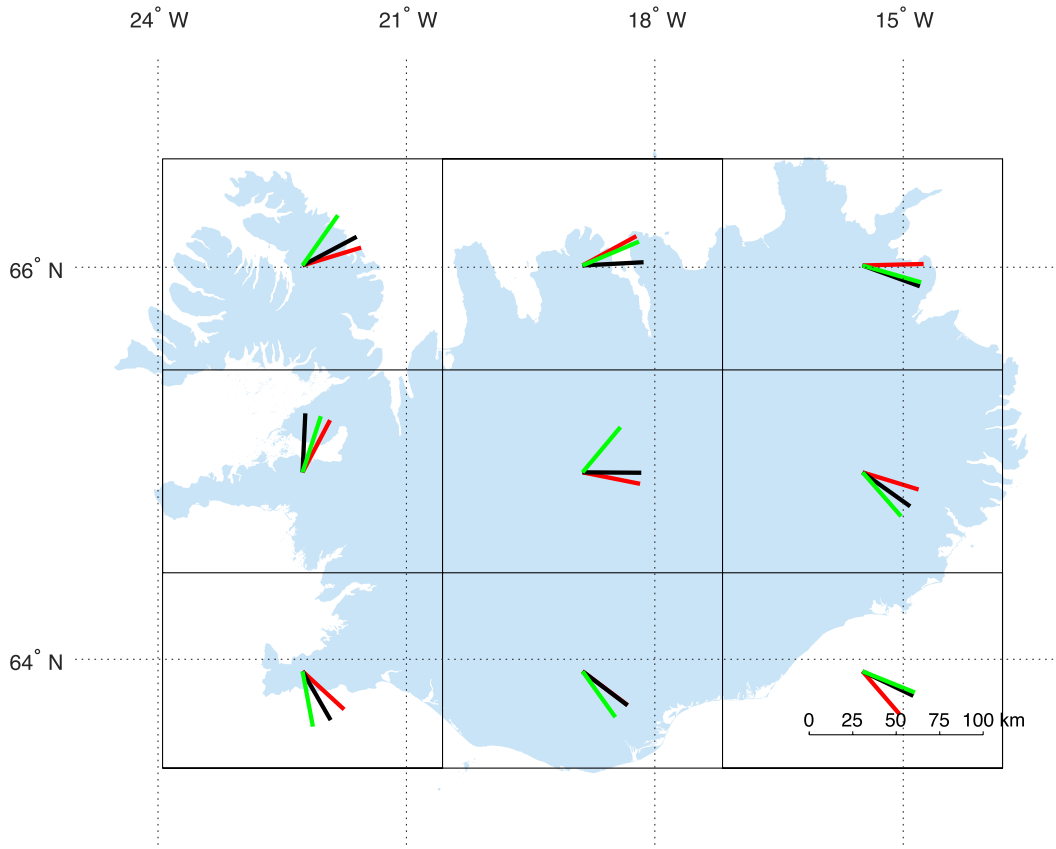


**Figure 7.** Map showing axes of maximum extensional strain in each of nine regions of Iceland, represented by the black boxes. Modeled axes are shown in black, based on the trial with the reference parameters, a rifting azimuth of 115° and the hotspot at 110 mm of element-normal dislocation. Axes derived directly from GPS velocities are shown in red. Axes from a model with just 10 mm of hotspot contribution and no consideration of rifting or fault interaction are shown in green.

95°. For the reference parameters, the mean deviatoric stress ratio is 0.75, with a mean of 0.6 in the top 5% of individual data set trials.

The top 5% of trials fitting the IMO seismicity data generally agree with the reference parameters but show an additional set of trials with a wide range of rifting azimuths (60°–145°) and no hotspot contribution. Western Hreppar shows the greatest improvement in the best fit trial as opposed to the reference parameters, with a best fit misfit of 38.3° as opposed to a misfit of 41.8° for the reference parameters (Figure 3), while the best fit trial shows slightly worse fit in the GORZ. For the reference parameters, the mean deviatoric stress ratio is 0.47, with a mean of 0.75 in the top 5% of individual data set trials. Both stress data sets identify permutations between $\sigma_1$ and $\sigma_2$ as the most common.

The reference parameters are contained within the top 5% of trials fitting GPS data alone, with an average misfit of 17.1°, 3.5° higher than the minimum average misfit of 13.6°. None of the nine regions considered had an angular misfit above 35° in the model run with the reference parameters (Figure 3 and Figure S8 in Supporting Information S1). Strain rate axes derived from both the model results and the observed velocities show a general pattern of more southerly trending extensional azimuths in Southern Iceland (Figure 7).

### 3.2. Additional Model Parameter Variations

In assessing the impacts of the older hotspot configuration, rift propagation, and fault opening, we focus on comparing the results to moment tensor axes derived from fault slip records (Karson et al., 2018), as the comparison data that is the most widely geographically distributed and sensitive to variability in the standard parameter range (Table 2).

**Table 2**
*Table Showing Lowest Average Angular Misfit in Comparison With the Karson et al. (2018) Data Set, for Each of the Additional Variations Added to the Model: Allowing All Faults to Open, Allowing Poorly Fit Faults to Open, Placing the Hotspot in Its Proposed Location as of 6 Ma (Martin et al., 2011), and Allowing Variable Remote Stress (H, Hotspot Contribution [mm/Year]; R, Rifting Azimuth; M, Average Angular Misfit)*

| | Fault slip derived (moment tensor axes, $n = 13$) | | |
|---|---|---|---|
| | H | R (°) | M (°) |
| All dikes | 50 | 110 | 36.1 |
| Dikes in poorly fit areas | 40 | 100 | 33.5 |
| Old hotspot | 50 | 100 | 39.6 |
| Variable remote stress | 10 | 105 | 36.7 |

To consider possible older faulting patterns, we ran trials varying the location of the hotspot based on two sets of rifting and hotspot contribution parameters. The average results from each of the top 5% of trials found the lowest average angular misfit of 39.2° at the modern-day location and the highest misfit of 43.1° at the 6 Ma location. For the additional model with the hotspot at its 6 Ma location (Figure S9 in Supporting Information S1) and a hypothetical fault representing rifting along the length of the SPRA, we ran trials based on the full suite of standard parameters. In comparison with a model with the same hotspot location and without the SPRA, the model showed improvements in the areas of Hegranes and Grenivík and worse fit in the areas of Tröllaskagi and Flateyjarskagi, leading to a very similar minimum average misfit, 0.3° higher (locations, Figure 1).

Allowing for less rifting stress at the propagating rift tips resulted in the lowest average angular misfit decreasing 0.1°–36.7° with 10 mm/year of hotspot contribution and a rifting azimuth of 105°, generally preferring a much lower hotspot contribution but similar rifting azimuth as the standard model. This suggests that a pattern of decreasing remote stress at distance from the hotspot largely replicates the influence of the hotspot itself, requiring only a very small hotspot contribution to obtain a strong fit with the comparison data.

When simulating dike intrusion, we found shifts in some regions as a result of only allowing poorly fit faults to open (defined in Section 2.3). For the moment tensor data derived from fault slip (Karson et al., 2018), the best fit standard parameters shifted slightly to 40 mm/year of element-normal dislocation on the hotspot and a 100° azimuth of rifting, and the lowest average angular misfit decreased from 36.8° to 33.5°. Less overall improvement was seen when allowing all faults to open. Improvement in the minimum angular misfit was largely due to improvements in Vopnafjörður, Grenivík, East Flateyjarskagi, and Akureyri (Figure 8).

## 4. Discussion

### 4.1. Standard Model

The lowest average angular misfit of 29.4° from a model with a rifting azimuth of 115° and a hotspot contribution of 110 mm/year suggests that stress applied in a direction similar to the NUVEL 1-A rifting azimuth of 105° (DeMets et al., 1994) and supplementary influence from the hotspot fits well with a variety of deformation indicators from Iceland in most regions. The top 5% of trials based on average angular misfit include rifting azimuths between 90° and 120° and a hotspot contribution between 20 and 130 mm/year. Overall, these deformation indicators suggest greater sensitivity to rifting azimuth than to hotspot contribution. For the reference model, the most common angular misfit by data point, including data points from all comparison data sets, is 20.6°. Within a three-dimensional space, this most common angular misfit translates to similarity in moment tensor, principal stress, and principal strain axis orientations between the model and comparison data. In addition, the resulting rakes for the reference model (Figure 5) show geographically widespread strike-slip faulting. This indicates that mechanical fault–hotspot interactions may explain a large part of faulting kinematics, and especially plate boundary-parallel strike-slip faulting in Iceland, using a simple representation of plate boundary stressing.

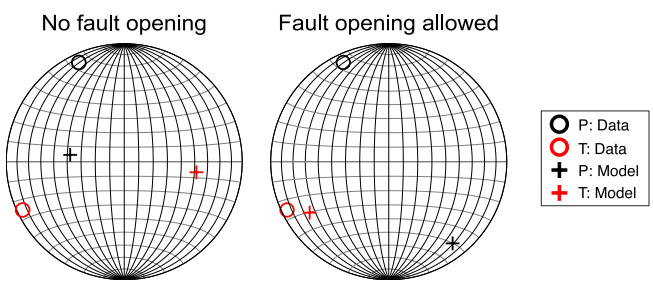


**Figure 8.** Stereonets show kinematic (P and T) axes for collected fault slip data and for model results using the reference parameters and comparison data for an example region, Grenivík, both with and without allowing fault opening.

### 4.2. Impact of Primary Tectonic Processes on Faulting Kinematics

Comparison of modeled deformation with different data sets largely shows good agreement with the NUVEL 1-A relative plate motion azimuth of 105° (DeMets et al., 1994), with additional complexity seen in some data sets. The Global CMT data and strain inferred from Icelandic GPS velocity field data collected 1993–2004 in ITRF2005 coordinates (Altamimi et al., 2007; Árnadóttir et al., 2009; Cardozo & Allmendinger, 2009; Dziewonski et al., 1981; Ekström et al., 2012) are each consistent with axes of maximum extension that are more southerly trending in Southern Iceland. A model run deriving the axis of the maximum extension rate from surface velocities due to hotspot

inflation alone, with no impact from fault interaction or plate boundary rifting, shows a very similar pattern of rotations clockwise from the NUVEL 1-A azimuth of 105° (Figure 7), suggesting that the inclusion of the hotspot accounts for much of this regional variation within the model. However, the trial parameters that best fit the CMT data feature a more southeasterly trending rifting azimuth (120°) than NUVEL 1-A, regardless of the intensity of the hotspot. This indicates either (a) a uniform remote stress tensor applied across all of Iceland may not be an appropriate description of tectonic forcing or (b) the inclusion of the hotspot as it is considered within our model may not be sufficient to account for the rotation of axes of maximum extension in Southern Iceland.

The data sets derived from fault slip were best fit over a range of possible hotspot contributions, with the exception of a subset of parameters that best fit the IMO seismicity data at no hotspot contribution, potentially because those earthquakes are located farther from the hotspot center and so feel its influence to a lesser extent (Table S4 in Supporting Information S1; Ziegler et al., 2016). Larger hotspot contributions also led to an increase in modeled sinistral faulting in northwest Iceland (Figure 5), consistent with observed fault slip as well as the rift propagation model proposed by Karson et al. (2018).

Our modeling of hotspot inflation, which appears at the Earth's surface as uplift and a radial pattern of horizontal velocities away from the hotspot center, gives results that are broadly similar to velocities predicted by models of glacial isostatic adjustment (GIA) for Iceland. Both our modeled hotspot inflation and GIA models result in a radial pattern of horizontal velocities away from Vatnajökull, due to the location of the center of the hotspot underneath this ice cap. This suggests that results supporting the inclusion of the hotspot would be similarly well-fit by models considering GIA. However, inclusion of dislocations applied to the hotspot elements also provides a good fit to fault slip records. While age constraints on fault activity are limited, fault slip records likely include some activity from before the current interglacial, which provides support for the validity of a hotspot model. In addition, other GIA models have predicted lower velocities, especially horizontally, than the velocities observed by GPS (Drouin & Sigmundsson, 2019). This indicates that our hotspot implementation may be best considered as a combined effect of contributions from both hotspot inflation and GIA.

The results based on stress tensor axes provide insight into the possibility of stress permutations between $\sigma_1$ and $\sigma_2$ as explanation for the presence of strike-slip faulting in Iceland, based on conjugate normal and strike-slip faults. Additional factors within Iceland, including crustal anisotropy and elastic rebound, could contribute to favoring localized perturbations in the stress field (Hu & Angelier, 2004; Plateaux et al., 2012). While we did not directly implement anisotropy or unloading effects within the model, allowing stress permutations in the assessment of model fit to principal stress axes provides a means of considering a potential impact of these processes. The identification of possible exchanges between steeply plunging $\sigma_1$ and $\sigma_2$ axes as the most common type of permutations within the top 5% of trials for stress tensor axes derived from both fault slip and earthquakes fits with this hypothesis (Plateaux et al., 2012).

### 4.3. Impact of Additional Model Complexity on Faulting Kinematics

The larger misfits that result from varying the location of the hotspot support modeling the hotspot in its proposed modern-day location, rather than its proposed position at 6 Ma (I. Bjarnason, 2008; Martin et al., 2011), suggest that the majority of fault kinematic data in Iceland are reflective of a more modern period. The results also support not including the SPRA, although some regions (Hegranes and Grenivík) showed improvement when considering this feature. This local improvement signals the possibility of a representation of older faulting kinematics within the slip record in select areas, related to a now abandoned oblique spreading zone, with a similar lack of age constraints to confirm any variability.

A gradient in the magnitude of applied remote stress was included in the model for the purpose of testing rifting propagation, or the idea that the propagation of the Northern Rift Zone to the north and the Eastern Rift Zone to the south creates block rotations, which are a primary factor driving strike-slip faulting in Iceland (Karson, 2017). Overall, changes as a result of this gradient introduced no significant improvement in model fit and the results do not strongly support the notion of rift propagation as a primary process influencing fault slip patterns, at least not as simulated in this way. However, more direct modeling of block rotations could provide additional insight into the possibility.

Misfit to moment tensor data derived from fault slip (Karson et al., 2018) improved as a result of allowing poorly fit faults to open, simulating dike intrusion. This improvement occurred primarily in the regions of Vopnafjörður,

Grenivík, East Flateyjarskagi, and to some extent in Akureyri, implying the influence of dike intrusion as an additional factor influencing fault kinematics in these regions (Figure 1 and Figure S9 in Supporting Information S1). We attempted to analyze whether these regions could have significantly more cumulative dike intrusion than other areas in Iceland by determining the proportion of measured dikes to measured faults and the average dike width in the Karson et al. (2018) data. However, there is uncertainty as to whether the structure types were comprehensively sampled, especially due to dike and fault data sets coming from different sources, and measurements of dike width were limited. There is also ambiguity in the relative timing of dike intrusion and faulting. Therefore, despite local improvement, we defined the standard model as allowing no opening on faults.

### 4.4. Analysis and Significance

Necessary simplifications of the modeling process (Text S1) could impact the results. However, although additional complexity could provide a more accurate modeled representation of Iceland, the goal of the modeling process was to see how much kinematic complexity can arise from a relatively simple mechanical model. This process allows for an understanding of what effect the inputs to the simple model have, which is a significant strength of the approach. Furthermore, no additional tests adding greater complexity to the model resulted in a universal model improvement, which is a continued argument for focusing on the standard model.

An additional possible complicating factor in comparing modeled and observed fault kinematics is the lack of constraints on the age of faulting in Iceland. In comparing model results to observations, we assume that deformation throughout the country, as represented in the slip data, GPS data, and recent earthquakes, is a response to a common stress field. Different regions might be dominated by faulting from different time periods more accurately represented by separate models and findings of both normal and strike-slip faulting within one region in the field could actually correspond to changed faulting kinematics during two different time periods (Karson et al., 2018). However, we would then expect a pattern visible in the field showing cross-cutting relationships between normal and strike-slip faults as well as multiple sets of slickenlines indicating a change in kinematics over time. Consistent patterns were not observed and at least some of the faults cut glacial or postglacial lavas (Karson et al., 2018). In addition, while models simulating older tectonic conditions suggest a potential difference, especially around Hegranes, these older parameters yield a generally good fit to modern earthquake data, modern GPS data, and fault slip data. Although it cannot be fully evaluated without more comprehensive age constraints, this supports the idea that much of the slip data in the field represents relatively modern faulting kinematics.

We find that mechanical fault–hotspot interaction may explain a large part of faulting kinematics, including widespread plate boundary-parallel strike-slip faulting. These results also show consistency across data sets derived from multiple sources, indicating that strike-slip faulting may continue to a significant extent in the modern-day stress field. This has important implications for our understanding of the Icelandic plate boundary system as well as potential seismic hazard in Iceland, especially outside the major transform zones. Although the major transform zones have been the source of the majority of the large magnitude ($M \geq 6$) historical earthquakes in Iceland (J. Ö. Bjarnason et al., 2016), our results help to better understand the potential for faulting in other areas of Iceland. In addition, our finding of an improved fit in some regions due to allowing dike intrusion has implications for the potential for enhanced volcanic activity in those areas, although we were not able to evaluate whether those regions are indeed more volcanically active.

This modeling is also significant for considering faulting processes along other Mid-Ocean Ridges, as those processes are difficult to observe on the seafloor. In addition, our work indicates the possibility that similar mechanical fault–hotspot interaction could occur in other hotspot–rift systems, like the Ethiopia/Afar hotspot underlying the East African Rift. Widespread strike-slip faulting has been found in the Afar triangle, although with fewer oblique mechanisms and with the added complication of a triple junction between multiple rifts (Abbate et al., 1995).

## 5. Conclusions

A simple model of faulting kinematics in Iceland, based only on an influence from the hotspot, uniaxial remotely applied stress to simulate rifting close to the NUVEL 1-A azimuth of 105°, and interactions among modeled faults, fits well with observed records of fault slip, seismicity, and geodetic deformation in Iceland and produces a significant amount of plate boundary-parallel strike-slip faulting. Increases in model complexity, particularly in

allowing fault opening, lead to reduced misfit in select regions but indicate no universal improvement. Fit is also relatively consistent across data types, including the geodetic and seismicity data that record contemporary deformation, suggesting that the fault slip data available may be largely representative of the modern stress field. The good fit of the simple model points to hotspot–fault–rifting interactions as a major driver of plate boundary-parallel strike-slip faulting, with a potential additional influence from GIA that may be convolved with our representation of the hotspot contribution. Results do not support a strong impact on faulting in Iceland from differences in rifting stress due to rift propagation. However, possible stress permutations between $\sigma_1$ and $\sigma_2$ are commonly identified in models that mimic rifting conditions close to those predicted by NUVEL 1-A, indicating that local perturbations to the stress field may also impact strike-slip faulting. These results provide a new understanding of the physical mechanisms driving faulting kinematics within Iceland outside the current active plate boundary.

## Data Availability Statement

All data used in this study were taken from the cited papers and/or their supplementary material (Árnadóttir et al., 2009; Bergerat et al., 1990; Dziewonski et al., 1981; Ekström et al., 2012; Gudmundsson et al., 1992; Karson et al., 2018; Plateaux et al., 2012; Ziegler et al., 2016). A Matlab Live Script and associated functions that can be used to run the same model comparison is available online at http://doi.org/10.5281/zenodo.3333886.

**Acknowledgments**
The authors thank Jeff Karson for helpful discussion and a thorough, informed review of the manuscript. The authors also thank editor Laurent Jolivet and an anonymous reviewer for additional helpful comments. This work was supported by funding from Smith College.

## References

Abbate, E., Passerini, P., & Zan, L. (1995). Strike-slip faults in a rift area: A transect in the Afar Triangle, East Africa. *Tectonophysics*, *241*, 67–97. https://doi.org/10.1016/0040-1951(94)00136-W

Ágústsdóttir, T., Woods, J., Greenfield, T., Green, R., White, R., Winder, T., et al. (2016). Strike-slip faulting during the 2014 Bárðarbunga–Holuhraun dike intrusion, central Iceland. *Geophysical Research Letters*, *43*, 1495–1503. https://doi.org/10.1002/2015GL067423

Allmendinger, R. W., Cardozo, N., & Fisher, D. M. (2011). *Structural geology algorithms*. Cambridge University Press.

Altamimi, Z., Collilieux, X., Legrand, J., Garayt, B., & Boucher, C. (2007). ITRF2005: A new release of the International Terrestrial Reference Frame based on time series of station positions and Earth Orientation Parameters. *Journal of Geophysical Research*, *112*, B09401. https://doi.org/10.1029/2007JB004949

Anderson, E. M. (1905). The dynamics of faulting. *Transactions of the Edinburgh Geological Society*, *8*, 387–402. https://doi.org/10.1144/transed.8.3.387

Árnadóttir, T., Lund, B., Jiang, W., Geirsson, H., Björnsson, H., Einarsson, P., & Sigurdsson, T. (2009). Glacial rebound and plate spreading: Results from the first countrywide GPS observations in Iceland. *Geophysical Journal International*, *177*(2), 691–716. https://doi.org/10.1111/j.1365-246X.2008.04059.x

Bergerat, F., Angelier, J., & Homberg, C. (2000). Tectonic analysis of the Husavik-Flatey Fault (Northern Iceland) and mechanics of an oceanic transform zone the Tjörnes Fracture Zone. *Tectonics*, *19*(6), 1161–1177. https://doi.org/10.1029/2000TC900022

Bergerat, F., Angelier, J., & Villemin, T. (1990). Fault systems and stress patterns on emerged oceanic ridges: A case study in Iceland. *Tectonophysics*, *179*(3–4), 183–197. https://doi.org/10.1016/0040-1951(90)90290-O

Bjarnason, I. (2008). An Iceland hotspot saga. *Jökull Journal*, *58*, 3–16.

Bjarnason, J. Ö., Einarsson, P., & Bessason, B. (2016). Iceland catastrophe insurance and earthquake risk assessment. Paper presented at International Workshop on Earthquakes in North Iceland. Retrieved from http://www.hac.is/wp-content/uploads/2016/05/Iceland-Catstrophe-Insurance-and-Earthquake-Risk-Assessment.pdf

Björnsson, A. (2008). Temperature of the Icelandic crust: Inferred from electrical conductivity, temperature surface gradient, and maximum depth of earthquakes. *Tectonophysics*, *447*, 136–141. https://doi.org/10.1016/j.tecto.2006.02.027

Cardozo, N., & Allmendinger, R. W. (2009). SSPX: A program to compute strain from displacement/velocity data. *Computers & Geosciences*, *35*(6), 1343–1357. https://doi.org/10.1016/j.cageo.2008.05.008

Cooke, M., & Dair, L. C. (2011). Simulating the recent evolution of the southern big bend of the San Andreas fault, Southern California. *Journal of Geophysical Research*, *116*, B04405. https://doi.org/10.1029/2010JB007835

Delano, J. E., Amos, C. B., Loveless, J. P., Rittenour, T. M., Sherrod, B. L., & Lynch, E. M. (2017). Influence of the megathrust earthquake cycle on upper-plate deformation in the Cascadia forearc of Washington State, USA. *Geology*, *45*(11), 1051–1054. https://doi.org/10.1130/G39070.1

DeMets, C., Gordon, R. G., Argus, D. F., & Stein, S. (1994). Effect of recent revisions to the geomagnetic reversal time scale on estimates of current plate motions. *Geophysical Research Letters*, *21*(20), 2191–2194. https://doi.org/10.1029/94GL02118

Drouin, V., & Sigmundsson, F. (2019). Countrywide observations of plate spreading and glacial isostatic adjustment in Iceland inferred by Sentinel-1 Radar Interferometry, 2015–2018. *Geophysical Research Letters*, *46*, 8046–8055. https://doi.org/10.1029/2019GL082629

Dziewonski, A. M., Chou, T. A., & Woodhouse, J. H. (1981). Determination of earthquake source parameters from waveform data for studies of global and regional seismicity. *Journal of Geophysical Research*, *86*(B4), 2825–2852. https://doi.org/10.1029/JB086iB04p02825

Einarsson, P. (2008). Plate boundaries, rifts and transforms in Iceland. *Jökull Journal*, *58*, 35–58.

Ekström, G., Nettles, M., & Dziewonski, A. M. (2012). The Global CMT project 2004–2010: Centroid-moment tensors for 13,107 earthquakes. *Physics of the Earth and Planetary Interiors*, *200–201*, 1–9. https://doi.org/10.1016/j.pepi.2012.04.002

Garcia, S., Angelier, J., Bergerat, F., Homberg, C., & Dauteuil, O. (2008). Influence of rift jump and excess loading on the structural evolution of Northern Iceland. *Tectonics*, *27*, TC1006. https://doi.org/10.1029/2006TC002029

Garcia, S., Arnaud, N. O., Angelier, J., Bergerat, F., & Homberg, C. (2003). Rift jump process in Northern Iceland since 10 Ma from $^{40}Ar/^{39}Ar$ geochronology. *Earth and Planetary Science Letters*, *214*(3–4), 529–544. https://doi.org/10.1016/S0012-821X(03)00400-X

Geuzaine, C., & Remacle, J.-F. (2009). Gmsh: A 3-D finite element mesh generator with built-in pre- and post-processing facilities. *International Journal for Numerical Methods in Engineering*, *79*(11), 1309–1331. https://doi.org/10.1002/nme.2579

Gudmundsson, A., Bergerat, F., Angelier, J., & Villemin, T. (1992). Extensional tectonics of southwest Iceland. *Bulletin de la Société géologique de France*, *5*, 561–570.

Gudmundsson, A., Friese, N., Andrew, R., Philipp, S. L., Ertl, G., & Letourneur, L. (2009). Effects of dyke emplacement and plate pull on mechanical interaction between volcanic systems and central volcanoes in Iceland. In T. Thordarson, S. Self, G. Larsen, S. K. Rowland, & A. Hoskuldsson (Eds.), *Studies in volcanology: The legacy of George Walker* (Vol. 2, pp. 331–347). IAVCEL.

Hanan, B. B., & Schilling, J.-G. (1997). The dynamic evolution of the Iceland mantle plume: The lead isotope perspective. *Earth and Planetary Science Letters*, *151*, 43–60. https://doi.org/10.1016/s0012-821x(97)00105-2

Hardarson, B. S., Fitton, J. G., Ellam, R. M., & Pringle, M. S. (1997). Rift relocation: A geochemical and geochronological investigation of a palaeo-rift in northwest Iceland. *Earth and Planetary Science Letters*, *153*, 181–196. https://doi.org/10.1016/s0012-821x(97)00145-3

Hjartardóttir, Á. R., Einarsson, P., Magnúsdóttir, S., Jonsdottir, Þ., & Brandsdóttir, B. (2015). Fracture systems of the Northern Volcanic Rift Zone, Iceland: An onshore part of the Mid-Atlantic plate boundary. *Geological Society - Special Publications*, *420*, 297–314. https://doi.org/10.1144/SP420.1

Hjartardóttir, Á. R., Einarsson, P., & Sigurdsson, H. (2009). The fissure swarm of the Askja volcanic system along the divergent plate boundary of N Iceland. *Bulletin of Volcanology*, *71*, 961.

Hjartarson, Á. (2003). *The Skagafjörður unconformity and its geological history*. University of Copenhagen.

Hu, J. C., & Angelier, J. (2004). Stress permutations: Three-dimensional distinct element analysis accounts for a common phenomenon in brittle tectonics. *Journal of Geophysical Research*, *109*, B09403. https://doi.org/10.1029/2003JB002616

Jóhannesson, H. (2014). *Geological map of Iceland, 1:600,000 [map]*. Icelandic Institute of Natural History.

Karson, J. A. (2017). The Iceland plate boundary zone: Propagating rifts, migrating transforms, and rift-parallel strike-slip faults. *Geochemistry, Geophysics, Geosystems*, *18*, 4043–4054. https://doi.org/10.1002/2017GC007045

Karson, J. A., Farrell, J. A., Chutas, L. A., Nanfito, A. F., Proett, J. A., Runnals, K. T., & Sæmundsson, K. (2018). Rift-parallel strike-slip faulting near the Iceland plate boundary zone: Implications for propagating rifts. *Tectonics*, *37*, 4567–4594. https://doi.org/10.1029/2018TC005206

Loveless, J. P. (2019). *tribem: Boundary element code using triangular dislocation elements in Matlab*. Zenodo. https://doi.org/10.5281/zenodo.3333886

Marrett, R. A., & Allmendinger, R. W. (1990). Kinematic analysis of fault-slip data. *Journal of Structural Geology*, *12*, 973–986. https://doi.org/10.1016/0191-8141(90)90093-e

Martin, E., Paquette, J. L., Bosse, V., Ruffet, G., Tiepolo, M., & Sigmarsson, O. (2011). Geodynamics of rift–plume interaction in Iceland as constrained by new $^{40}Ar/^{39}Ar$ and in situ U–Pb zircon ages. *Earth and Planetary Science Letters*, *311*(1–2), 28–38. https://doi.org/10.1016/j.epsl.2011.08.036

Morgan, W. J., & Morgan, J. P. (2007). Plate velocities in the hotspot reference frame. *Special Paper of the Geological Society of America*, *430*(04), 65–78. https://doi.org/10.1130/2007.2430(04)

Plateaux, R., Bergerat, F., Béthoux, N., Villemin, T., & Gerbault, M. (2012). Implications of fracturing mechanisms and fluid pressure on earthquakes and fault slip data in the east Iceland rift zone. *Tectonophysics*, *581*, 19–34. https://doi.org/10.1016/j.tecto.2012.01.013

Rögnvaldsson, S. T., Gudmundsson, A., & Slunga, R. (1998). Seismotectonic analysis of the Tjörnes Fracture Zone, an active transform fault in north Iceland. *Journal of Geophysical Research*, *103*(B12), 30117–30129. https://doi.org/10.1029/98JB02789

Sigurdsson, O. (2005). *GLIMS glacier database*. National Snow and Ice Data Center. https://doi.org/10.7265/N5V98602

Thomas, A. L. (1993). *Poly3D: A three-dimensional, polygonal element, displacement discontinuity boundary element computer program with applications to fractures, faults, and cavities in the Earth's crust (PhD Thesis)*. Stanford University.

Wolfe, C. J., Bjarnason, I. T., VanDecar, J. C., & Solomon, S. C. (1997). Seismic structure of the Iceland mantle plume. *Nature*, *385*, 245–247. https://doi.org/10.1038/385245a0

Ziegler, M., Rajabi, M., Heidlbach, O., Hersir, G., Ágústsson, K., Árnadóttir, S., & Zang, A. (2016). The stress pattern of Iceland. *Tectonophysics*, *674*, 101–113. https://doi.org/10.1016/j.tecto.2016.02.008

## Erratum

In the originally published version of this article, a previous draft of Figure 6 was included. A corrected version of Figure 6 has been added to the article, and this version may be considered the authoritative version of record.